

CERN-PH-EP-2012-002
08 January 2012

Measurement of event background fluctuations for charged particle jet reconstruction in Pb–Pb collisions at $\sqrt{s_{\text{NN}}} = 2.76$ TeV

ALICE Collaboration *

Abstract

The effect of event background fluctuations on charged particle jet reconstruction in Pb–Pb collisions at $\sqrt{s_{\text{NN}}} = 2.76$ TeV has been measured with the ALICE experiment. The main sources of non-statistical fluctuations are characterized based purely on experimental data with an unbiased method, as well as by using single high p_t particles and simulated jets embedded into real Pb–Pb events and reconstructed with the anti- k_t jet finder. The influence of a low transverse momentum cut-off on particles used in the jet reconstruction is quantified by varying the minimum track p_t between 0.15 GeV/ c and 2 GeV/ c . For embedded jets reconstructed from charged particles with $p_t > 0.15$ GeV/ c , the uncertainty in the reconstructed jet transverse momentum due to the heavy-ion background is measured to be 11.3 GeV/ c (standard deviation) for the 10% most central Pb–Pb collisions, slightly larger than the value of 11.0 GeV/ c measured using the unbiased method. For a higher particle transverse momentum threshold of 2 GeV/ c , which will generate a stronger bias towards hard fragmentation in the jet finding process, the standard deviation of the fluctuations in the reconstructed jet transverse momentum is reduced to 4.8–5.0 GeV/ c for the 10% most central events. A non-Gaussian tail of the momentum uncertainty is observed and its impact on the reconstructed jet spectrum is evaluated for varying particle momentum thresholds, by folding the measured fluctuations with steeply falling spectra.

*See Appendix A for the list of collaboration members

1 Introduction

High energy heavy-ion collisions explore strongly interacting matter under extreme conditions of energy density, where lattice QCD predicts a phase transition to a new state of matter above a critical value of about $1 \text{ GeV}/\text{fm}^3$ [1]. In this new state, called the Quark-Gluon Plasma (QGP), quarks and gluons rather than hadrons are expected to be the dominant degrees of freedom over length scales larger than that of a nucleon. Experiments studying the collision of heavy nuclei at high energy at both the Relativistic Heavy Ion Collider (RHIC) [2, 3, 4, 5], and recently at the Large Hadron Collider (LHC) [6, 7, 8, 9], have made several key observations that point to the formation of a hot, dense and strongly coupled system, possibly the QGP.

Hard (large momentum transfer Q^2) probes are well calibrated tools to study the properties of the matter created in such collisions. The scattered partons generated in a hard momentum exchange are created in the initial stages of the heavy-ion collision, with production rates that are calculable using perturbative QCD, which can be compared to the same measurements in proton-proton collisions. The scattered partons then propagate through the medium, where their fragmentation into observed jets of hadrons is expected to be modified relative to the vacuum case by interactions with the medium (*jet quenching*) [10, 11]. This modification of parton fragmentation provides sensitive observables to study properties of the created matter.

Jet quenching has been observed at RHIC [12, 13, 14, 15] and at the LHC [16] via the measurement of high p_t hadron inclusive production and correlations, which are observed to be strongly suppressed in central A–A collisions compared to a scaled pp reference. These high p_t hadron observables have been the major tool for measuring the energy loss of hard scattered partons and thereby the properties of the medium, but they provide only indirect and biased information on the parton evolution in the medium. The aim of full jet reconstruction is to measure jet modifications due to energy loss in an unbiased way [17, 18]. Already first measurements of reconstructed jets in heavy-ion collisions at the LHC showed an energy imbalance between back-to-back dijets, which is attributed to jet quenching [9, 19].

Jet reconstruction in the complex environment of a heavy-ion collision requires a quantitative understanding of background-induced fluctuations of the measured jet signal and the effects of the underlying heavy-ion event on the jet finding process itself. Here, region-to-region background fluctuations are the main source of jet energy or momentum uncertainty and can have a large impact on jet structure observables, such as the fraction of energy inside the jet core or the shape of the jet, and will distort the measured jet energy balance even in the absence of medium effects [20].

In this paper the measurement of jet transverse momentum fluctuations due to the background in heavy-ion collisions is reported and its sources are identified, based on jet reconstruction using charged particles with varying minimum track p_t . For this purpose three methods are employed to probe the measured Pb–Pb events: fixed area (*rigid*) cones placed randomly in the acceptance, the simulation of high- p_t single tracks or full jets from pp collisions. Rigid cones enable the identification of contributions to the fluctuations in an unbiased fashion, while single tracks and embedded jets explore the interplay between the jet finding process, the underlying event, and the jet fragmentation pattern.

2 Detector Description and Track Selection

The data presented here were collected by the ALICE experiment [21] in the first Pb–Pb run of the LHC in November 2010, at a collision energy of $\sqrt{s_{\text{NN}}} = 2.76 \text{ TeV}$. This analysis is based on minimum-bias events, triggered by two forward VZERO counters and the Silicon Pixel Detector (SPD)[22]. A description of the minimum-bias trigger can be found in [6]. The VZERO trigger counters are forward scintillator detectors covering a pseudo-rapidity range of $2.8 < \eta < 5.1$ (V0A) and $-3.7 < \eta < -1.7$ (V0C). The sum of VZERO amplitudes is also used as a measure of event centrality [23]. The SPD

consists of two silicon pixel layers at a radial distance to the beam line of $r = 3.9$ cm and $r = 7.6$ cm.

To ensure a uniform track acceptance in pseudo-rapidity η , only events whose primary vertex lies within ± 8 cm from the center of the detector along the beam line are used, resulting in 13.3 M minimum-bias Pb–Pb events for this analysis.

Charged particle tracking is carried out using the Time Projection Chamber (TPC) [24] and the Inner Tracking System (ITS) [22], located in the central barrel of the ALICE experiment within a 0.5 T solenoidal magnetic field and covering the full azimuth within pseudo-rapidity $|\eta| < 0.9$. The ITS consists of six cylindrical layers of silicon detectors, with distances from the beam-axis between $r = 3.9$ cm and $r = 43$ cm. The ITS layers measure track points close to the primary vertex, with the two innermost layers (SPD) providing a precise measurement of the primary vertex position. The TPC, a cylindrical drift detector surrounding the ITS, is the main tracking detector in ALICE. The TPC inner radius is 85 cm and the outer radius is 247 cm, with longitudinal coverage $-250 < z < 250$ cm. It provides a uniformly high tracking efficiency for charged particles. The high precision of the ITS and the large radial lever arm of the TPC provide a good momentum resolution for combined (*global*) tracks.

For this dataset the ITS has significantly non-uniform efficiency as a function of azimuthal angle ϕ and pseudo-rapidity η . In order to obtain high and uniform tracking efficiency together with good momentum resolution, two different track populations are utilized: (i) tracks containing at least one space-point reconstructed in one of the two innermost layers of the ITS (78% of all accepted tracks), and (ii) accepted tracks that lack the position information close to the beam-line. Here, the primary vertex is added to the fit of the track which modifies the reconstructed curvature of the charged track in the magnetic field. Since the majority of the tracks originates from the primary vertex this constraint improves the momentum resolution. Both track types have transverse momentum resolution of $\sigma(p_t)/p_t \approx 1\%$ at 1 GeV/c. For the majority of tracks the resolution at $p_t = 50$ GeV/c is $\sigma(p_t)/p_t \approx 10\%$, only tracks having fewer than three reconstructed space points in the ITS (about 6% of the total population) have a resolution at 50 GeV/c of $\sigma(p_t)/p_t \approx 20\%$.

Tracks are accepted for $p_t > 0.15$ GeV/c and $|\eta| < 0.9$. The tracking efficiency at $p_t = 0.15$ GeV/c is 50%, increasing to 90% at 1 GeV/c and above. Tracks with measured $p_t > 100$ GeV/c are accepted at the tracking stage, but jets containing them are rejected from the analysis to reduce the influence of fake tracks and limited tracking resolution at very high p_t .

3 Jet Reconstruction and Background Subtraction

Charged particle jet reconstruction and estimation of the background employ the sequential recombination algorithms anti- k_t and k_t from the FastJet package [25]. The clustering starts with the list of tracks that satisfy the quality, acceptance, and p_t -cuts, with no pre-clustering or grouping of tracks. A list of jet candidates (anti- k_t) or clusters (k_t) is generated, with direction and transverse momentum given by the p_t -weighted average of (η, ϕ) of the individual constituents and the scalar sum of their p_t , respectively. The distance parameter that determines the terminating condition for the clustering is chosen as $R = 0.4$, which is a common value for reconstruction of jets in heavy-ion collisions [18, 9, 26]. As proposed in [27], the clusters found by the k_t algorithm are used to estimate the event-wise background p_t -density per unit area, ρ , defined as the median value of the ratio $p_t^{\text{rec}}/A^{\text{rec}}$ for all considered k_t -clusters. A^{rec} is the area of the reconstructed cluster in the (η, ϕ) -plane calculated by the active ghost area method of FastJet [28], with a ghost area of 0.005. To minimize the influence of the track acceptance interval on ρ , only reconstructed clusters with $|\eta| < 0.5$ have been used. In addition, the two clusters with the largest p_t^{rec} (leading) in the full acceptance of $|\eta| < 0.9$ are excluded from the calculation of the median to further reduce the influence of true jets on the background estimate [29]. The jet population reconstructed by the anti- k_t algorithm is used as signal jets. Their p_t is corrected for the background p_t -density in each event using the jet area $A^{\text{jet,rec}}$ with $p_t^{\text{jet}} = p_t^{\text{jet,rec}} - \rho \cdot A^{\text{jet,rec}}$. Signal jets are only considered for $|\eta| < 0.5$.

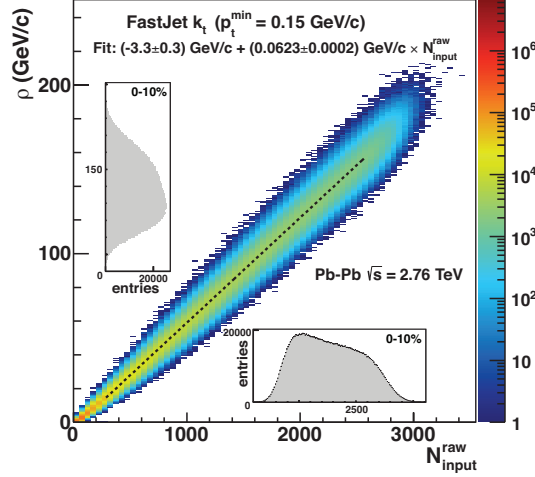


Figure 1: Dependence of charged particle background p_t density ρ on uncorrected multiplicity of tracks used for jet finding ($|\eta| < 0.9$). The dotted line is a linear fit to the centroids in each multiplicity bin. The insets show the projected distributions of ρ and raw multiplicity for the 10% most central events.

p_t^{\min} (GeV/c)	$\langle \rho \rangle$ (GeV/c)	$\sigma(\rho)$ (GeV/c)
0-10%		
0.15	138.32 ± 0.02	18.51 ± 0.01
1.00	59.30 ± 0.01	9.27 ± 0.01
2.00	12.28 ± 0.01	3.29 ± 0.01
50-60%		
0.15	12.05 ± 0.01	3.41 ± 0.01
1.00	4.82 ± 0.01	1.77 ± 0.01
2.00	4.41 ± 0.05	0.92 ± 0.04

Table 1: Average and standard deviation of the event-wise charged particle p_t density ρ for three choices of minimum particle p_t and two centrality bins. The quoted uncertainties are purely statistical.

The average transverse momentum of tracks $\langle p_t \rangle$ and the total charged multiplicity are global observables that are closely related to the value of ρ , though the determination of ρ uses varying phase-space intervals (with typical areas in the (η, ϕ) -plane of πR^2) and suppresses hard jet contributions by using the median of the distribution. Figure 1 shows the correlation between ρ and the uncorrected multiplicity of tracks with $|\eta| < 0.9$. The linear increase corresponds to an uncorrected $\langle p_t \rangle$ of about 0.7 GeV/c per accepted charged track. Both $\langle p_t \rangle$ and multiplicity, and thus also the background p_t density, strongly depend on the minimum p_t threshold (p_t^{\min}) applied for tracks used as input to the jet finding. To minimize the bias on jet fragmentation, a value of $p_t^{\min} = 0.15$ GeV/c is preferred. In addition, $p_t^{\min} = 1$ and 2 GeV/c are investigated to facilitate comparisons to other experiments and to Monte-Carlo generators in a region of constant and high tracking efficiency. The mean ρ over all events and its standard deviation is given for different p_t^{\min} and two centralities in Table 1. As expected, the mean background p_t density decreases for larger p_t^{\min} , for central collisions and $p_t^{\min} = 2$ GeV/c it is reduced by an order of magnitude. As one can see in the insets of Figure 1 and the standard deviation in Table 1, the spread of ρ for the 10% most central events is considerable, underlining the importance of the event-by-event background subtraction.

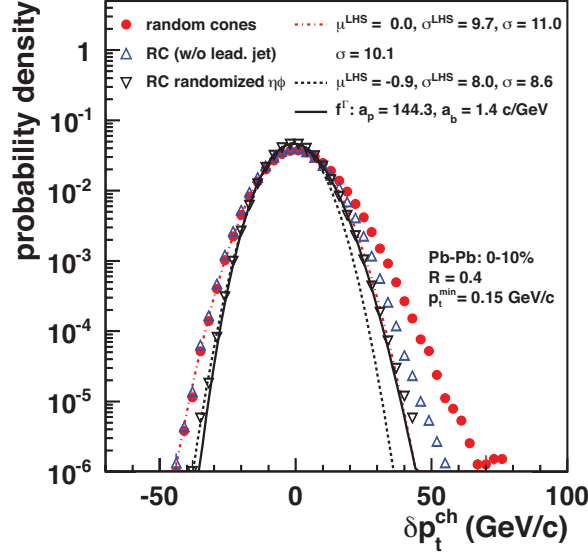


Figure 2: δp_t of random cones in the 10% most central Pb–Pb events for the three types of random cone probes with $p_t^{\min} = 0.15$ GeV/c. A Gaussian fit to the left-hand-side and its extrapolation to positive δp_t are shown for measured Pb–Pb events and for randomized Pb–Pb events (μ^{LHS} and σ^{LHS} in GeV/c). The solid line is a fit to the δp_t distribution for the randomized events with a Γ distribution shifted to zero (Equation 2) as approximation for the shape in case of independent particle emission.

4 Sources of Background Fluctuations

To study the sources of background fluctuations in an unbiased way that is not influenced by a particular choice of jet finder, a single rigid cone with radius $R = 0.4$ is placed in each reconstructed event at random ϕ and η , with centroid lying within $|\eta| < 0.5$. The background fluctuations are characterized by calculating the difference of the scalar sum of all track p_t in the cone and the expected background:

$$\delta p_t = \sum_i p_{t,i} - A \cdot \rho, \quad (1)$$

where $A = \pi R^2$.

The rigid random cone (RC) area and position are not influenced by the event, so that it provides a sampling of the event structure at the typical scale of a jet, but independent of biases induced by the choice of a particular jet finding algorithm. The RC measurements will be compared to the embedding of jet-like objects, that is directly relevant to the measurement of the inclusive jet spectrum with a specific choice of jet finder.

To characterize the δp_t distribution the standard deviation, $\sigma(\delta p_t)$, is utilized. In addition, a Gaussian distribution with mean μ^{LHS} and standard deviation σ^{LHS} is iteratively fit to the distribution within $[\mu^{\text{LHS}} - 3\sigma^{\text{LHS}}, \mu^{\text{LHS}} + 0.5\sigma^{\text{LHS}}]$, i.e. to the left-hand-side. The σ^{LHS} of the fit provides the lower limit on the magnitude of the fluctuations and is used to characterize shape differences between the positive and negative tails of the distribution, by extrapolating the Gaussian distribution to positive δp_t .

Various sources contribute to background fluctuations in a heavy-ion event, including: (i) random, uncorrelated (Poissonian) fluctuations of particle number and momentum; (ii) region-to-region correlated variations of the momentum density, induced by detector effects, e.g. a non-uniform efficiency, and by the heavy-ion collision itself, e.g. by variation of the eccentricity of the nuclear overlap for collisions with finite impact parameter.

The measured δp_t distribution for random cones in the 10% most central Pb–Pb events is shown in

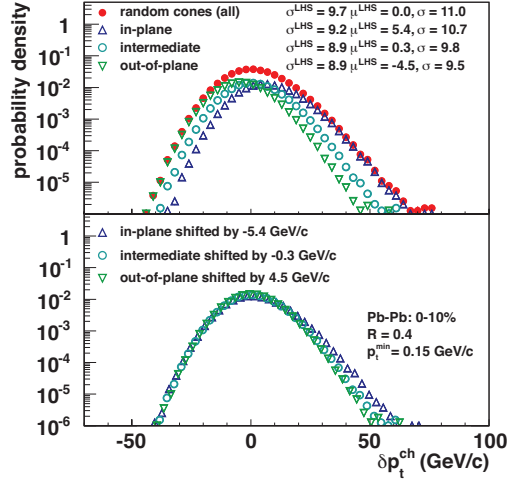


Figure 3: δp_t distribution for random cones, averaged over the full azimuth and separated for three bins of random cone azimuthal orientations with respect to the measured event plane. In the bottom panel the distributions have been shifted to zero using the mean of the left-hand-side Gaussian fit (μ^{LHS}).

Figure 2. The distribution is peaked near zero, illustrating the agreement of the background estimate via k_t -clusters and that due to random sampling of the event. The distribution exhibits an asymmetric shape with a tail to the right-hand-side of the distribution, which is also reflected in the difference between the standard deviation of the full distribution of $\sigma(\delta p_t) = 11.0 \text{ GeV}/c$ and the Gaussian width of the left-hand-side $\sigma^{\text{LHS}}(\delta p_t) = 9.6 \text{ GeV}/c$.

To further differentiate random and correlated sources of fluctuations, three variations of the random cone method are employed: (i) sampling of measured Pb–Pb events, (ii) sampling of measured Pb–Pb events, but avoiding overlap with the leading jet candidate in the event after background subtraction by requiring a distance $D = 1.0$ in (η, ϕ) between the random cone direction and the jet axis, and (iii) sampling of Pb–Pb events in which the (η, ϕ) direction of the tracks has been randomized within the acceptance, which destroys all correlations in the event. Figure 2 shows that when avoiding the leading jet candidate to suppress upward fluctuations, e.g. due to a hard process, the tail to the right-hand-side is already significantly reduced.

Note that, even for the case of purely statistical fluctuations, the distribution is not expected to be symmetric or to follow a Gaussian shape on the right-hand-side, since the shapes of the underlying single particle p_t and multiplicity distributions are not Gaussian. In the case of uncorrelated particle emission a Γ -distribution provides a more accurate description of the event-wise $\langle p_t \rangle$ fluctuations [30]. This also holds for δp_t distributions, which are similar to a measurement of $\langle p_t \rangle$ fluctuations in a limited interval of phase space. Taking into account the subtraction of the average background the functional form of the probability distribution of δp_t for independent particle emission can be written:

$$f^\Gamma(\delta p_t) = A \cdot a_b / \Gamma(a_p) \cdot (a_b \delta p_t + a_p)^{a_p - 1} \cdot e^{-(a_b \delta p_t + a_p)}. \quad (2)$$

This corresponds to a Γ -distribution with mean shifted from a_p/a_b to zero and standard deviation $\sigma = \sqrt{a_p}/a_b$. As seen in Figure 2 this functional form provides a good approximation of the δp_t distribution for randomized events, corresponding to uncorrelated emission. In this case the distribution is also narrower on the left-hand-side. This points to the presence of correlated region-to-region fluctuations in addition to purely statistical fluctuations and those expected from hard processes.

One source of region-to-region variation in the background p_t density is the initial anisotropy of the nuclear overlap for finite impact parameter collisions, which translates via the collective expansion of the medium into an anisotropy in momentum space [7, 31] with respect to the symmetry plane of the

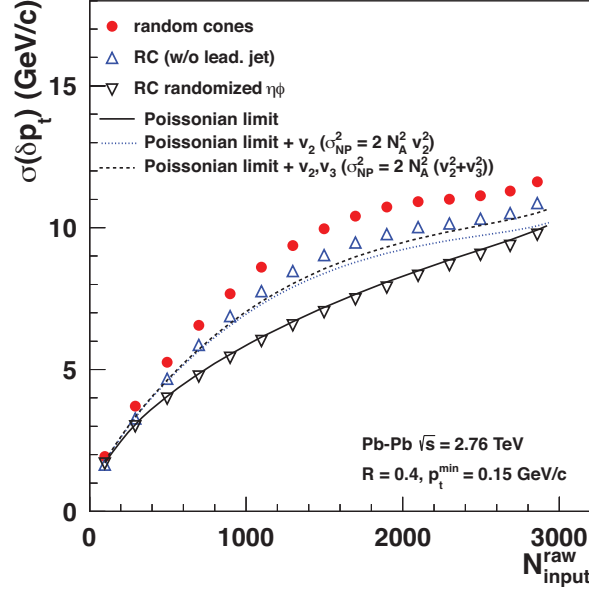


Figure 4: Dependence of the standard deviation of the δp_t distributions on uncorrected charged particle multiplicity, compared to the limit derived from the measured track p_t spectrum (Equation 3) and from additional elliptic and triangular flow contributions (Equation 4). $R = 0.4$, $p_t^{\min} = 0.15$ GeV/c.

collision. The event plane direction can be calculated using the azimuthal distribution of all accepted tracks within each event, which is dominated by soft particle production. The final state hadron azimuthal distribution with respect to the reaction plane of the event, is characterized by a Fourier expansion where the leading term is the second moment, called elliptic flow v_2 . In addition to the geometry driven even harmonics (mainly v_2), odd flow components (e.g. v_3) driven by initial state fluctuations can modify the azimuthal distribution within the event [32].

To explore the effect on background fluctuations of azimuthal orientation relative to the reaction plane, the δp_t distribution from random cone sampling is studied as a function of the azimuthal orientation of the cone axis, ϕ , relative to the reconstructed event plane orientation, ψ_{RP} . Three bins are chosen; the out-of-plane orientation where the azimuthal angle between the reconstructed event plane and the cone axis is $> 60^\circ$, the in-plane orientation where this angle is $< 30^\circ$, and the intermediate orientation where the angle is between 30 and 60° . The distributions of δp_t for random cones averaged over the full azimuth and for the three different orientations are shown in Figure 3. It can be seen that, for out-of-plane cones, the most probable background p_t density is smaller by almost 5 GeV/c relative to the azimuthally averaged estimate of ρ , with opposite effect in-plane. This shift scales with the average flow and the background p_t density for a given centrality ($\propto v_2 \cdot \rho$), and is seen to be sizable in central events, though discrimination of the event plane orientations is limited by finite event-plane resolution [33] and possible biases due to hard jets. The decreasing width of left-hand-side Gaussian is qualitatively consistent with the expectation from reduced particle number fluctuations out-of-plane compared to in-plane. For a visual comparison of their shape, the distributions have been shifted such that the centroid of the left-hand-side Gaussian fit is zero (see Figure 3). Notably, the left-hand-side of the distribution appears similar for all orientations of the random cones to the event-plane. The random cones distributed in-plane show a more pronounced tail to the right-hand-side, compared to out-of-plane. This may point to a dependence of the jet spectrum on the orientation relative to the reaction plane, though further systematic studies are needed to assess biases in the event plane determination due to jet production and possible auto-correlations. For the measurement of the inclusive jet spectrum the correction via an event-plane dependent ρ will reduce the influence of even flow components on the average reconstructed jet momentum, but its systematic precision is limited by the finite event-plane resolution.

The width of the δp_t distribution due to purely random fluctuations can be estimated from the measured single particle p_t spectrum via [18]:

$$\sigma(\delta p_t) = \sqrt{N_A \cdot \sigma^2(p_t) + N_A \cdot \langle p_t \rangle^2}. \quad (3)$$

Here, N_A is the expected number of tracks in the cone area A for a given event centrality or multiplicity class, $\langle p_t \rangle$ the average p_t and $\sigma(p_t)$ the standard deviation of the track p_t spectrum. Local variations of the average multiplicity, $\langle p_t \rangle$, or $\sigma(p_t)$, lead to additional fluctuations. These region-to-region variations can be induced e.g. by (mini-)jets, where the particle p_t spectrum is considerably harder than for the global event average, and by collective flow. Uncorrelated non-Poissonian (NP) fluctuations can be added to Equation 3 knowing their standard deviation, e.g. for additional region-to-region variation of the average multiplicity:

$$\sigma(\delta p_t) = \sqrt{N_A \cdot \sigma^2(p_t) + (N_A + \sigma_{\text{NP}}^2(N_A)) \cdot \langle p_t \rangle^2}. \quad (4)$$

Figure 4 shows the comparison of the multiplicity dependence of $\sigma(\delta p_t)$ for the three different types of random cones. The distribution of purely statistical fluctuations given by Equation 3 well describes the randomized events. Also shown are two parameterizations following Equation 4. Additional multiplicity fluctuations due to elliptic flow are approximated from the p_t -integrated v_2 values measured by ALICE for different centralities [7] as $\sigma_{\text{NP}}^2(N_A) \approx 2v_2^2 N_A^2$. This approximate inclusion of v_2 -effects accounts qualitatively for the larger fluctuations in mid central collisions compared to the randomized events and the deviation from a \sqrt{N} -increase. The random cone sampling with an anti-bias on the leading jet has, by construction, a reduced standard deviation and is close to the parameterization of elliptic flow. Taking into account also region-to-region fluctuations from triangular flow, v_3 , is of particular importance in central events where it reaches a similar magnitude as v_2 [32]. The contribution of v_3 can be added in quadrature ($\sigma_{\text{NP}}^2(N_A) \approx 2N_A^2(v_2^2 + v_3^2)$) since the second and the third harmonic are not correlated via a common plane of symmetry [32], for simplicity v_3 has been approximated by a constant value of $v_3 = 2.4\%$. As expected, the inclusion of v_3 can account partially for the difference to the randomized event in the most central events. In the comparison one has to consider that in practice the contribution from hard processes to the right-hand-side tail cannot be cleanly separated from (soft) upward multiplicity fluctuations induced by flow. In addition, the approximate description of flow effects following Equation 4 does not take into account any flow-correlated changes of $\langle p_t \rangle$ and $\sigma(p_t)$.

The track reconstruction efficiency affects the total multiplicity and the shape of the measured p_t -spectrum at low p_t . Using Equation 3, the change of the uncorrelated fluctuations due to finite efficiency can be estimated from the efficiency corrected p_t -spectrum in each centrality bin. This procedure suggests that, for $p_t^{\text{min}} = 0.15$ GeV/c, there is an increase of the standard deviation by 5.4–6.0%, depending on centrality. The complete correction requires the knowledge of all correlations within the heavy-ion event and is beyond the scope of the present study.

5 Background Fluctuations in Jet Reconstruction

The measured jet spectrum in heavy-ion collisions is affected over the entire p_t range by background fluctuations, especially due to the large and asymmetric tail towards positive δp_t . For the measurement of the inclusive jet cross section, background fluctuations can only be corrected on a statistical basis via unfolding. Such background fluctuations are evaluated using embedding and reconstruction of a probe with identical jet algorithm and parameters as those applied to the data analysis, to account for the jet-finder-specific response to the heavy-ion background.

In the present study, two probes are embedded into the Pb–Pb events measured by ALICE: (i) single high- p_t tracks at various p_t , and (ii) pp jet events generated using PYTHIA [34] followed by a detailed

simulation of the full detector response. Jet candidates are reconstructed from the event using the anti- k_t algorithm with $R = 0.4$ and matched to the embedded probe, by either finding the single track in it, or by requiring that the p_t of the embedded tracks within the reconstructed jet sum up to at least 50% of the original probe jet transverse momentum (p_t^{probe}). The difference between the reconstructed, background subtracted jet and the embedded probe is then given, similar to Equation 1, by [29, 35]:

$$\delta p_t = p_t^{\text{jet,rec}} - A^{\text{jet,rec}} \cdot \rho - p_t^{\text{probe}}. \quad (5)$$

The response may depend on the jet finder, its settings, and the properties of the embedded probe, such as p_t^{probe} , area, and fragmentation pattern. In particular the insensitivity to the latter is essential for a robust and unbiased reconstruction of jets in heavy-ion collisions, where the fragmentation pattern is potentially modified relative to that in pp collisions, and is indeed the observable of interest.

The δp_t distributions measured for each of the methods are shown in Figure 5. Here, the focus is on high p_t^{probe} ($> 60 \text{ GeV}/c$), where the efficiency of matching the embedded probe to the reconstructed jet approaches unity. The results are very similar to the random cone method, including the presence of an asymmetric tail to the right-hand-side of the distribution. The standard deviations, however, show a small increase compared to the random cone method, which is largest for jet embedding (see Table 2). The increase may be due to sensitivity of the jet finder to back-reaction, e.g. the stability of the probe area and jet direction after embedding. The single particle embedding can be considered as extreme fragmentation leading to rather rigid cones with stable area πR^2 , while in the case of true pp-jets the probe and reconstructed area may differ, depending on the fragmentation pattern. In addition the finite jet area resolution due to the size of the ghost area has to be taken into account [29]. With a ghost area of 0.005 a compromise between reasonable jet area resolution and computing time and memory consumption was chosen. In the case of track embedding at high p_t , the jet area resolution fully accounts for the difference of $200 \text{ MeV}/c$ observed in the standard deviation.

The broadening of the δp_t distribution for jets with $p_t^{\text{min}} = 0.15 \text{ GeV}/c$, as seen in Figure 5, has been investigated more closely. The additional left-hand-side structure is caused by probe jets with large area ($A^{\text{probe}} > 0.6$) that are split in the heavy-ion event into two separate objects of smaller size. Jets with a large area ($A > 0.6$) are only formed by the anti- k_t algorithm in exceptional cases, where there are two hard cores at distance close to R [36]. It is also seen in Figure 5 that, with increasing p_t^{min} , the deviations on the left-hand-side in the case of jet embedding become more pronounced, suggesting that the jet-splitting is an effect of hard fragmentation.

In the determination of δp_t fluctuations as described above, the probes have been embedded into an event population recorded with a minimum-bias trigger. However, the requirement of a hard process biases the population towards more central (small impact parameter) collisions, due to nuclear geometry. Correction of this effect for centrality bins of 10% width, generates a negligible increase of the fluctuations ($< 0.1 \text{ GeV}/c$). The full centrality dependence of the fluctuations is given via the standard deviation of the distributions and for different p_t^{min} cuts in Table 3.

The increase of the p_t^{min} cut on the input tracks for jet finding reduces the background fluctuations, due to the smaller influence of statistical and soft region-to-region fluctuations. This is observed in Figure 5 when the p_t^{min} is varied from 0.15 to $2 \text{ GeV}/c$. A p_t^{min} of $2 \text{ GeV}/c$ reduces the standard deviation by more than a factor of two compared to $0.15 \text{ GeV}/c$. Soft region-to-region fluctuations that dominate the left-hand-side of the distribution are reduced by a factor of three (see Table 2). A high p_t^{min} significantly reduces the impact of fluctuations in the jet spectrum (see Table 4). However, it may also introduce a bias in the jet reconstruction towards hard fragmentation.

To estimate the influence of the observed fluctuations on the jet measurement, a power law spectrum starting at $p_t = 4 \text{ GeV}/c$ has been folded with a Gaussian of width $\sigma^{\text{Gauss}} = 11 \text{ GeV}/c$ ($5 \text{ GeV}/c$) and with the measured δp_t distributions for $p_t^{\text{min}} = 0.15 \text{ GeV}/c$ ($2 \text{ GeV}/c$). The yield increase relative to the

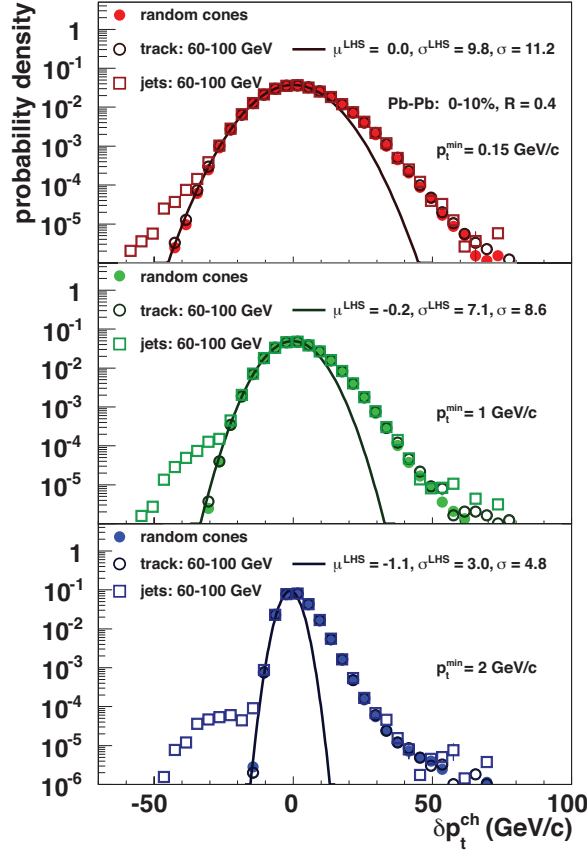


Figure 5: δp_t distribution of charged particles for jet reconstruction with the three methods in the 10% most central Pb–Pb events for $p_t^{\min} = 0.15$ GeV/c, 1 GeV/c, and 2 GeV/c.

unsmeared spectrum in one high p_t -bin for the most central collisions is given in Table 4. For the different probes, they agree within the uncertainties given by the statistical fluctuations in the tails of the δp_t -distributions; about a factor of ten increase for $p_t^{\min} = 0.15$ GeV/c and a 30% effect for $p_t^{\min} = 2$ GeV/c. Minor differences in the standard deviation as well as the left-hand-side differences have no sizable effect on the spectral shape after folding. The difference between smearing with the full δp_t and with a Gaussian distribution illustrates the strong influence of the right-hand-side tail, which must be taken into account in the analysis of background fluctuation effects on jet reconstruction. The extracted values naturally depend on the choice of the input spectrum, so, in addition to the power law, a jet spectrum for pp collisions at $\sqrt{s_{NN}} = 2.76$ TeV extracted from PYTHIA simulations has been used. These studies indicate that the increase of yield due to background fluctuations falls below 50% for reconstructed charged jets in the region of $p_t \approx 100 \pm 15$ GeV/c (60 ± 10 GeV/c) for $p_t^{\min} = 0.15$ GeV/c (2 GeV/c). Repeating the exercise with a Gaussian smearing of a $\sigma^{\text{Gauss}} = 11$ GeV/c and with the δp_t distribution of random cones avoiding the leading jet for $p_t^{\min} = 0.15$ GeV/c leads, as expected, to a reduced influence of the tail. Here, the relative yield increase falls below 50% in the range of $p_t \approx 75 \pm 10$ GeV/c. The employed input spectra do not consider the geometrical limitation on the number of jets that can be reconstructed within the acceptance for a single event [37]. This effect also limits the extraction of jet spectra at lower p_t via unfolding.

6 Summary

The first detailed study of event background fluctuations for jet reconstruction using charged particles in Pb–Pb collisions at the LHC has been presented. The standard deviation of the fluctuations in the

	σ (GeV/c)	σ^{LHS} (GeV/c)	μ^{LHS} (GeV/c)
$p_t^{\text{min}} = 0.15$ GeV/c			
random cones	10.98 ± 0.01	9.65 ± 0.02	-0.04 ± 0.03
track emb.	11.19 ± 0.01	9.80 ± 0.02	0.00 ± 0.03
jet emb.	11.34 ± 0.02	9.93 ± 0.06	0.06 ± 0.09
$p_t^{\text{min}} = 1$ GeV/c			
random cones	8.50 ± 0.01	7.08 ± 0.01	-0.22 ± 0.02
track emb.	8.61 ± 0.01	7.11 ± 0.01	-0.25 ± 0.02
jet emb.	8.78 ± 0.02	7.25 ± 0.04	-0.08 ± 0.08
$p_t^{\text{min}} = 2$ GeV/c			
random cones	4.82 ± 0.01	3.41 ± 0.01	-0.01 ± 0.01
track emb.	4.88 ± 0.01	3.05 ± 0.01	-0.92 ± 0.01
jet emb.	5.03 ± 0.01	3.52 ± 0.01	0.01 ± 0.02

Table 2: Background fluctuations in central events. Comparison of the Gaussian fit to the left-hand-side of the δp_t -distributions and the standard deviation in central Pb–Pb collisions for the three different methods and for the three p_t^{min} -cuts. The quoted uncertainties are purely statistical.

Centrality Class	p_t^{min} (GeV/c)		
	0.15	1.0	2.0
	$\sigma(\delta p_t)$ (GeV/c)		
0-10%	11.19 ± 0.01	8.61 ± 0.01	4.88 ± 0.01
10-20%	10.19 ± 0.01	7.67 ± 0.01	4.29 ± 0.01
20-30%	8.46 ± 0.01	6.35 ± 0.01	3.58 ± 0.01
30-40%	6.51 ± 0.01	4.93 ± 0.01	2.68 ± 0.01
40-50%	4.71 ± 0.01	3.63 ± 0.01	1.95 ± 0.01
50-60%	3.28 ± 0.01	2.61 ± 0.01	1.41 ± 0.01
60-70%	2.22 ± 0.01	1.70 ± 0.01	0.95 ± 0.01
70-80%	1.48 ± 0.01	1.01 ± 0.01	0.62 ± 0.01

Table 3: Centrality dependence of fluctuations. Standard deviation of δp_t distributions and statistical uncertainty for different centrality bins and p_t^{min} cuts using the track embedding probe.

$f(p_t)$ folded with	relative yield for $p_t = 60 - 68$ GeV/c		
δp_t	RC	tracks	jets
$p_t^{\text{min}} = 0.15$ GeV/c	9.8 ± 1.7	11.4 ± 1.1	10.9 ± 3.4
$p_t^{\text{min}} = 2$ GeV/c	1.30 ± 0.02	1.31 ± 0.02	1.65 ± 0.25
Gauss			
$\sigma = 11$ GeV/c		1.82 ± 0.04	
$\sigma = 5$ GeV/c		1.05 ± 0.01	

Table 4: Yield modification for power law spectrum. Relative yield in the bin $p_t = 60 - 68$ GeV/c for a power law spectrum ($f(p_t) = 0.7/(0.7 + p_t^5)$ and $p_t > 4$ GeV/c), folded with the different δp_t distributions for 0-10% centrality and with a Gaussian, where the width is similar to the standard deviation of the δp_t distributions.

10% most central events is $\sigma = (10.98 \pm 0.01)$ GeV/ c within a rigid cone of $R = 0.4$ and for a low p_t cut-off of 0.15 GeV/ c . It has been shown that the non-statistical sources of fluctuations are driven in part by the anisotropy of the particles emitted from the collision (elliptic and triangular flow). The variation of multiplicity in different orientations with respect to the event plane, induces shifts in the background-subtracted jet p_t even for central Pb–Pb-collisions.

The anti- k_t jet finder response for charged particle jet reconstruction has a modest dependence on the method used to characterize the fluctuations. For embedded, simulated pp-jets the standard deviation increases to (11.34 ± 0.02) GeV/ c . In addition, certain rare fragmentation patterns in pp are likely to be split in the heavy-ion environment leading to minor effects in the background response. The observed differences between the two types of embedded probes (namely single tracks and pp jets) do not indicate a strong sensitivity of the reconstructed anti- k_t jet spectrum on fragmentation. The case of a strong broadening of the jet due to medium effects has not been considered here.

The use of reconstructed charged particles down to $p_t^{\min} = 0.15$ GeV/ c allows a comparison of the impact of background fluctuations with a minimal bias on hard fragmentation in jet finding to the case with increased bias ($p_t^{\min} \geq 1$ GeV/ c). The observed reduction of the standard deviation to $\sigma = (4.82 \pm 0.01)$ GeV/ c for the unbiased sampling and $p_t^{\min} = 2$ GeV/ c is driven by the smaller number fluctuations and the reduced influence of soft region-to-region fluctuations.

The asymmetric shape of the δp_t distribution with a tail towards positive fluctuations has a large impact on the jet measurement, compared to purely Gaussian fluctuations, though the role of signal jets contributing to the tail has to be considered. Using different assumptions on the shape of the true jet spectrum it is found that for $p_t^{\min} = 0.15$ GeV/ c fluctuations can have a large influence on the charged jet yield for transverse momenta up to 100 ± 15 GeV/ c .

Acknowledgements

The ALICE collaboration would like to thank all its engineers and technicians for their invaluable contributions to the construction of the experiment and the CERN accelerator teams for the outstanding performance of the LHC complex.

The ALICE collaboration acknowledges the following funding agencies for their support in building and running the ALICE detector:

Calouste Gulbenkian Foundation from Lisbon and Swiss Fonds Kidagan, Armenia;

Conselho Nacional de Desenvolvimento Científico e Tecnológico (CNPq), Financiadora de Estudos e Projetos (FINEP), Fundação de Amparo à Pesquisa do Estado de São Paulo (FAPESP);

National Natural Science Foundation of China (NSFC), the Chinese Ministry of Education (CMOE) and the Ministry of Science and Technology of China (MSTC);

Ministry of Education and Youth of the Czech Republic;

Danish Natural Science Research Council, the Carlsberg Foundation and the Danish National Research Foundation;

The European Research Council under the European Community’s Seventh Framework Programme;

Helsinki Institute of Physics and the Academy of Finland;

French CNRS-IN2P3, the ‘Region Pays de Loire’, ‘Region Alsace’, ‘Region Auvergne’ and CEA, France;

German BMBF and the Helmholtz Association;

General Secretariat for Research and Technology, Ministry of Development, Greece;

Hungarian OTKA and National Office for Research and Technology (NKTH);

Department of Atomic Energy and Department of Science and Technology of the Government of India;

Istituto Nazionale di Fisica Nucleare (INFN) of Italy;

MEXT Grant-in-Aid for Specially Promoted Research, Japan;

Joint Institute for Nuclear Research, Dubna;
National Research Foundation of Korea (NRF);
CONACYT, DGAPA, México, ALFA-EC and the HELEN Program (High-Energy physics Latin-American–European Network);
Stichting voor Fundamenteel Onderzoek der Materie (FOM) and the Nederlandse Organisatie voor Wetenschappelijk Onderzoek (NWO), Netherlands;
Research Council of Norway (NFR);
Polish Ministry of Science and Higher Education;
National Authority for Scientific Research - NASR (Autoritatea Națională pentru Cercetare Științifică - ANCS);
Federal Agency of Science of the Ministry of Education and Science of Russian Federation, International Science and Technology Center, Russian Academy of Sciences, Russian Federal Agency of Atomic Energy, Russian Federal Agency for Science and Innovations and CERN-INTAS;
Ministry of Education of Slovakia;
Department of Science and Technology, South Africa;
CIEMAT, EELA, Ministerio de Educación y Ciencia of Spain, Xunta de Galicia (Consellería de Educación), CEADEN, Cubaenergía, Cuba, and IAEA (International Atomic Energy Agency);
Swedish Research Council (VR) and Knut & Alice Wallenberg Foundation (KAW);
Ukraine Ministry of Education and Science;
United Kingdom Science and Technology Facilities Council (STFC);
The United States Department of Energy, the United States National Science Foundation, the State of Texas, and the State of Ohio.

References

- [1] F. Karsch and E. Laermann. Thermodynamics and in-medium hadron properties from lattice QCD. In Rudolph C. Hwa, editor, *Quark-Gluon Plasma 3*, pages 1–59. World Scientific, 2003.
- [2] John Adams et al. Experimental and theoretical challenges in the search for the quark gluon plasma: The STAR collaboration’s critical assessment of the evidence from RHIC collisions. *Nucl. Phys.*, A757:102–183, 2005.
- [3] K. Adcox et al. Formation of dense partonic matter in relativistic nucleus nucleus collisions at RHIC: Experimental evaluation by the PHENIX collaboration. *Nucl. Phys.*, A757:184–283, 2005.
- [4] I. Arsene et al. Quark Gluon Plasma and Color Glass Condensate at RHIC? The perspective from the BRAHMS experiment. *Nucl. Phys.*, A757:1–27, 2005.
- [5] B. B. Back et al. The PHOBOS perspective on discoveries at RHIC. *Nucl. Phys.*, A757:28–101, 2005.
- [6] K. Aamodt et al. Charged-particle multiplicity density at mid-rapidity in central Pb-Pb collisions at $\sqrt{s_{NN}} = 2.76$ TeV. *Phys. Rev. Lett.*, 105(25):252301, December 2010.
- [7] K. Aamodt et al. Elliptic flow of charged particles in Pb-Pb collisions at 2.76 TeV. *Phys. Rev. Lett.*, 105(25):252302, December 2010.
- [8] Serguei Chatrchyan et al. Dependence on pseudorapidity and centrality of charged hadron production in PbPb collisions at a nucleon-nucleon centre-of-mass energy of 2.76 TeV. *JHEP*, 08:141, 2011.
- [9] Georges Aad et al. Observation of a Centrality-Dependent Dijet Asymmetry in Lead-Lead Collisions at $\sqrt{s_{NN}} = 2.76$ TeV with the ATLAS Detector at the LHC. *Phys.Rev.Lett.*, 105:252303, 2010.
- [10] Miklos Gyulassy and Michael Plumer. Jet quenching in dense matter. *Phys. Lett.*, B243:432–438, 1990.

- [11] R. Baier, Yuri L. Dokshitzer, Alfred H. Mueller, S. Peigne, and D. Schiff. Radiative energy loss and p_T broadening of high-energy partons in nuclei. *Nucl.Phys.*, B484:265–282, 1997.
- [12] K. Adcox et al. Suppression of Hadrons with Large Transverse Momentum in Central Au+Au Collisions at $\sqrt{s_{NN}} = 130$ GeV. *Phys. Rev. Lett.*, 88:022301, 2002.
- [13] Stephen Scott Adler et al. Suppressed π^0 Production at Large Transverse Momentum in Central Au+Au Collisions at $\sqrt{s_{NN}} = 200$ GeV. *Phys. Rev. Lett.*, 91:072301, 2003.
- [14] J. Adams et al. Transverse Momentum and Collision Energy Dependence of High p_T Hadron Suppression in Au+Au Collisions at Ultrarelativistic Energies. *Phys. Rev. Lett.*, 91:172302, 2003.
- [15] John Adams et al. Evidence from d+Au measurements for final-state suppression of high p_T hadrons in Au+Au collisions at RHIC. *Phys. Rev. Lett.*, 91:072304, 2003.
- [16] K. Aamodt et al. Suppression of Charged Particle Production at Large Transverse Momentum in Central Pb–Pb Collisions at $\sqrt{s_{NN}} = 2.76$ TeV. *Phys. Lett.*, B696:30–39, 2011.
- [17] Carlos A. Salgado and Urs Achim Wiedemann. Medium modification of jet shapes and jet multiplicities. *Phys.Rev.Lett.*, 93:042301, 2004.
- [18] B. Alessandro et al. ALICE: Physics performance report, volume II. *J. Phys.*, G32:1295–2040, 2006.
- [19] Serguei Chatrchyan et al. Observation and studies of jet quenching in PbPb collisions at nucleon-nucleon center-of-mass energy = 2.76 TeV. *Phys. Rev.*, C84:024906, 2011.
- [20] Matteo Cacciari, Gavin P. Salam, and Gregory Soyez. Fluctuations and asymmetric jet events in PbPb collisions at the LHC. *Eur. Phys. J.*, C71:1692, 2011.
- [21] K. Aamodt et al. The ALICE experiment at the CERN LHC. *JINST*, 0803:S08002, 2008.
- [22] K. Aamodt et al. Alignment of the ALICE Inner Tracking System with cosmic-ray tracks. *JINST*, 5:P03003, 2010.
- [23] K. Aamodt et al. Centrality dependence of the charged-particle multiplicity density at mid-rapidity in Pb-Pb collisions at $\sqrt{s_{NN}} = 2.76$ TeV. *Phys. Rev. Lett.*, 106:032301, 2011.
- [24] J. Alme, Y. Andres, H. Appelshauser, S. Bablok, N. Bialas, et al. The ALICE TPC, a large 3-dimensional tracking device with fast readout for ultra-high multiplicity events. *Nucl.Instrum.Meth.*, A622:316–367, 2010.
- [25] Matteo Cacciari and Gavin P. Salam. Dispelling the N^3 myth for the k_t jet-finder. *Phys. Lett.*, B641:57–61, 2006.
- [26] Sevil Salur. First Direct Measurement of Jets in $\sqrt{s_{NN}} = 200$ GeV Heavy Ion Collisions by STAR. *Eur. Phys. J.*, C61:761–767, 2009.
- [27] Matteo Cacciari and Gavin P. Salam. Pileup subtraction using jet areas. *Phys. Lett.*, B659:119–126, 2008.
- [28] Matteo Cacciari, Gavin P. Salam, and Gregory Soyez. The Catchment Area of Jets. *JHEP*, 04:005, 2008.
- [29] Matteo Cacciari, Juan Rojo, Gavin P. Salam, and Gregory Soyez. Jet Reconstruction in Heavy Ion Collisions. *Eur.Phys.J.*, C71:1539, 2011.
- [30] M.J. Tannenbaum. The distribution function of the event-by-event average p_T for statistically independent emission. *Phys.Lett.*, B498:29–34, 2001.
- [31] Jean-Yves Ollitrault. Anisotropy as a signature of transverse collective flow. *Phys.Rev.*, D46:229–245, 1992.
- [32] K. Aamodt et al. Higher harmonic anisotropic flow measurements of charged particles in Pb-Pb collisions at $\sqrt{s_{NN}} = 2.76$ TeV. *Phys.Rev.Lett.*, 107:032301, 2011.
- [33] J. Bielcikova, S. Esumi, K. Filimonov, S. Voloshin, and J.P. Wurm. Elliptic flow contribution to two particle correlations at different orientations to the reaction plane. *Phys.Rev.*, C69:021901, 2004.
- [34] Torbjorn Sjostrand, Stephen Mrenna, and Peter Skands. PYTHIA 6.4 physics and manual. *JHEP*,

05:026, 2006.

- [35] P.M. Jacobs. Background Fluctuations in Heavy Ion Jet Reconstruction. *Nucl. Phys.*, A855:299–302, 2011.
- [36] Matteo Cacciari, Gavin P. Salam, and Gregory Soyez. The Anti- k_t jet clustering algorithm. *JHEP*, 0804:063, 2008.
- [37] Gabriel de Barros. Inclusive Distribution of Fully Reconstructed Jets in Heavy Ion Collisions at RHIC: Status Report. 2011. Proceedings for PANIC 2011, to appear in AIP conference series.

A The ALICE Collaboration

B. Abelev⁶⁹, J. Adam³⁴, D. Adamová⁷⁴, A.M. Adare¹²⁰, M.M. Aggarwal⁷⁸, G. Aglieri Rinella³⁰, A.G. Agocs⁶⁰, A. Agostinelli¹⁹, S. Aguilar Salazar⁵⁶, Z. Ahammed¹¹⁶, N. Ahmad¹⁴, A. Ahmad Masoodi¹⁴, S.U. Ahn^{64,37}, A. Akindinov⁴⁶, D. Aleksandrov⁸⁹, B. Alessandro⁹⁵, R. Alfaro Molina⁵⁶, A. Alici^{96,30,9}, A. Alkin², E. Almaráz Aviña⁵⁶, T. Alt³⁶, V. Altini^{28,30}, S. Altinpinar¹⁵, I. Altsybeev¹¹⁷, C. Andrei⁷¹, A. Andronic⁸⁶, V. Anguelov⁸³, J. Anielski⁵⁴, C. Anson¹⁶, T. Antičić⁸⁷, F. Antinori¹⁰⁰, P. Antonioli⁹⁶, L. Aphecetche¹⁰², H. Appelshäuser⁵², N. Arbor⁶⁵, S. Arcelli¹⁹, A. Arend⁵², N. Armesto¹³, R. Arnaldi⁹⁵, T. Aronsson¹²⁰, I.C. Arsene⁸⁶, M. Arslandok⁵², A. Asryan¹¹⁷, A. Augustinus³⁰, R. Averbeck⁸⁶, T.C. Awes⁷⁵, J. Äystö³⁸, M.D. Azmi¹⁴, M. Bach³⁶, A. Badalá⁹⁷, Y.W. Baek^{64,37}, R. Bailhache⁵², R. Bala⁹⁵, R. Baldini Ferroli⁹, A. Baldisseri¹², A. Baldit⁶⁴, F. Baltasar Dos Santos Pedrosa³⁰, J. Bán⁴⁷, R.C. Baral⁴⁸, R. Barbera²⁴, F. Barile²⁸, G.G. Barnaföldi⁶⁰, L.S. Barnby⁹¹, V. Barret⁶⁴, J. Bartke¹⁰⁴, M. Basile¹⁹, N. Bastid⁶⁴, B. Bathen⁵⁴, G. Batigne¹⁰², B. Batyunya⁵⁹, C. Baumann⁵², I.G. Bearden⁷², H. Beck⁵², I. Belikov⁵⁸, F. Bellini¹⁹, R. Bellwied¹¹⁰, E. Belmont-Moreno⁵⁶, S. Beole²⁶, I. Berceau⁷¹, A. Bercuci⁷¹, Y. Berdnikov⁷⁶, D. Berenyi⁶⁰, C. Bergmann⁵⁴, D. Berzano⁹⁵, L. Betev³⁰, A. Bhasin⁸¹, A.K. Bhati⁷⁸, N. Bianchi⁶⁶, L. Bianchi²⁶, C. Bianchin²², J. Bielčík³⁴, J. Bielčíková⁷⁴, A. Bilandzic⁷³, F. Blanco¹¹⁰, F. Blanco⁷, D. Blau⁸⁹, C. Blume⁵², M. Boccioni³⁰, N. Bock¹⁶, A. Bogdanov⁷⁰, H. Bøggild⁷², M. Bogolyubsky⁴³, L. Boldizsár⁶⁰, M. Bombara³⁵, J. Book⁵², H. Borel¹², A. Borissov¹¹⁹, S. Bose⁹⁰, F. Bossú^{30,26}, M. Botje⁷³, S. Böttger⁵¹, B. Boyer⁴², P. Braun-Munzinger⁸⁶, M. Bregant¹⁰², T. Breitner⁵¹, M. Broz³³, R. Brun³⁰, E. Bruna^{120,26,95}, G.E. Bruno²⁸, D. Budnikov⁸⁸, H. Buesching⁵², S. Bufalino^{26,95}, K. Bugaiev², O. Busch⁸³, Z. Buthelezi⁸⁰, D. Caballero Orduna¹²⁰, D. Caffarri²², X. Cai⁴⁰, H. Caines¹²⁰, E. Calvo Villar⁹², P. Camerini²⁰, V. Canoa Roman^{8,1}, G. Cara Romeo⁹⁶, F. Carena³⁰, W. Carena³⁰, N. Carlin Filho¹⁰⁷, F. Carminati³⁰, C.A. Carrillo Montoya³⁰, A. Casanova Díaz⁶⁶, M. Caselle³⁰, J. Castillo Castellanos¹², J.F. Castillo Hernandez⁸⁶, E.A.R. Casula²¹, V. Catanescu⁷¹, C. Cavicchioli³⁰, J. Cepila³⁴, P. Cerello⁹⁵, B. Chang^{38,123}, S. Chapeland³⁰, J.L. Charvet¹², S. Chattopadhyay⁹⁰, S. Chattopadhyay¹¹⁶, M. Cherney⁷⁷, C. Cheshkov^{30,109}, B. Cheynis¹⁰⁹, E. Chiavassa⁹⁵, V. Chibante Barroso³⁰, D.D. Chinellato¹⁰⁸, P. Chochula³⁰, M. Chojnacki⁴⁵, P. Christakoglou^{73,45}, C.H. Christensen⁷², P. Christiansen²⁹, T. Chujo¹¹⁴, S.U. Chung⁸⁵, C. Cicalo⁹³, L. Cifarelli^{19,30}, F. Cindolo⁹⁶, J. Cleymans⁸⁰, F. Coccetti⁹, J.-P. Coffin⁵⁸, F. Colamaria²⁸, D. Colella²⁸, G. Conesa Balbastre⁶⁵, Z. Conesa del Valle^{30,58}, P. Constantin⁸³, G. Contin²⁰, J.G. Contreras⁸, T.M. Cormier¹¹⁹, Y. Corrales Morales²⁶, P. Cortese²⁷, I. Cortés Maldonado¹, M.R. Cosentino^{68,108}, F. Costa³⁰, M.E. Cotallo⁷, E. Crescio⁸, P. Crochet⁶⁴, E. Cruz Alaniz⁵⁶, E. Cuautle⁵⁵, L. Cunqueiro⁶⁶, A. Dainese^{22,100}, H.H. Dalsgaard⁷², A. Danu⁵⁰, K. Das⁹⁰, D. Das⁹⁰, I. Das^{90,42}, A. Dash^{48,108}, S. Dash^{41,95}, S. De¹¹⁶, A. De Azevedo Moregula⁶⁶, G.O.V. de Barros¹⁰⁷, A. De Caro^{25,9}, G. de Cataldo⁹⁴, J. de Cuveland³⁶, A. De Falco²¹, D. De Gruttola²⁵, H. Delagrangé¹⁰², E. Del Castillo Sanchez³⁰, A. Deloff¹⁰¹, V. Demanov⁸⁸, N. De Marco⁹⁵, E. Dénes⁶⁰, S. De Pasquale²⁵, A. Deppman¹⁰⁷, G. D Erasmo²⁸, R. de Rooij⁴⁵, D. Di Bari²⁸, T. Dietel⁵⁴, C. Di Giglio²⁸, S. Di Liberto⁹⁹, A. Di Mauro³⁰, P. Di Nezza⁶⁶, R. Diviá³⁰, Ø. Djuvsland¹⁵, A. Dobrin^{119,29}, T. Dobrowolski¹⁰¹, I. Domínguez⁵⁵, B. Dönigus⁸⁶, O. Dordic¹⁸, O. Driga¹⁰², A.K. Dubey¹¹⁶, L. Ducroux¹⁰⁹, P. Dupieux⁶⁴, A.K. Dutta Majumdar⁹⁰, M.R. Dutta Majumdar¹¹⁶, D. Elia⁹⁴, D. Emschermann⁵⁴, H. Engel⁵¹, H.A. Erdal³², B. Espagnon⁴², M. Estienne¹⁰², S. Esumi¹¹⁴, D. Evans⁹¹, G. Eyyubova¹⁸, D. Fabris^{22,100}, J. Faivre⁶⁵, D. Falchieri¹⁹, A. Fantoni⁶⁶, M. Fasel⁸⁶, R. Fearick⁸⁰, A. Fedunov⁵⁹, D. Fehlker¹⁵, L. Feldkamp⁵⁴, D. Felea⁵⁰, G. Feofilov¹¹⁷, A. Fernández Téllez¹, A. Ferretti²⁶, R. Ferretti²⁷, J. Figiel¹⁰⁴, M.A.S. Figueredo¹⁰⁷, S. Filchagin⁸⁸, R. Fini⁹⁴, D. Finogeev⁴⁴, F.M. Fionda²⁸, E.M. Fiore²⁸, M. Floris³⁰, S. Foertsch⁸⁰, P. Foka⁸⁶, S. Fokin⁸⁹, E. Fragiaco⁹⁸, M. Fragkiadakis⁷⁹, U. Frankenfeld⁸⁶, U. Fuchs³⁰, C. Furget⁶⁵, M. Fusco Girard²⁵, J.J. Gaardhøje⁷², M. Gagliardi²⁶, A. Gago⁹², M. Gallio²⁶, D.R. Gangadharan¹⁶, P. Ganoti⁷⁵, C. Garabatos⁸⁶, E. Garcia-Solis¹⁰, I. Garishvili⁶⁹, J. Gerhard³⁶, M. Germain¹⁰², C. Geuna¹², A. Gheata³⁰, M. Gheata³⁰, B. Ghidini²⁸, P. Ghosh¹¹⁶, P. Gianotti⁶⁶, M.R. Girard¹¹⁸, P. Giubellino³⁰, E. Gladysz-Dziadus¹⁰⁴, P. Glässel⁸³, R. Gomez¹⁰⁶, E.G. Ferreira¹³, L.H. González-Trueba⁵⁶, P. González-Zamora⁷, S. Gorbunov³⁶, A. Goswami⁸², S. Gotovac¹⁰³, V. Grabski⁵⁶, L.K. Graczykowski¹¹⁸, R. Grajcarek⁸³, A. Grelli⁴⁵, C. Grigoras³⁰, A. Grigoras³⁰, V. Grigoriev⁷⁰, S. Grigoryan⁵⁹, A. Grigoryan¹²¹, B. Grinyov², N. Grion⁹⁸, P. Gros²⁹, J.F. Grosse-Oetringhaus³⁰, J.-Y. Grossiord¹⁰⁹, R. Grosso³⁰, F. Guber⁴⁴, R. Guernane⁶⁵, C. Guerra Gutierrez⁹², B. Guerzoni¹⁹, M. Guilbaud¹⁰⁹, K. Gulbrandsen⁷², T. Gunji¹¹³, A. Gupta⁸¹, R. Gupta⁸¹, H. Gutbrod⁸⁶, Ø. Haaland¹⁵, C. Hadjidakis⁴², M. Haiduc⁵⁰, H. Hamagaki¹¹³, G. Hamar⁶⁰, B.H. Han¹⁷, L.D. Hanratty⁹¹, A. Hansen⁷², Z. Harmanova³⁵, J.W. Harris¹²⁰, M. Hartig⁵², D. Hasegan⁵⁰, D. Hatzifotiadou⁹⁶, A. Hayrapetyan^{30,121}, S.T. Heckel⁵², M. Heide⁵⁴, H. Helstrup³², A. Hergelegiu⁷¹, G. Herrera Corral⁸, N. Herrmann⁸³, K.F. Hetland³², B. Hicks¹²⁰, P.T. Hille¹²⁰, B. Hippolyte⁵⁸, T. Horaguchi¹¹⁴, Y. Hori¹¹³, P. Hristov³⁰, I. Hřivnáčová⁴², M. Huang¹⁵, S. Huber⁸⁶,

T.J. Humanic¹⁶, D.S. Hwang¹⁷, R. Ichou⁶⁴, R. Ilkaev⁸⁸, I. Ilkiv¹⁰¹, M. Inaba¹¹⁴, E. Incani²¹, G.M. Innocenti²⁶, P.G. Innocenti³⁰, M. Ippolitov⁸⁹, M. Irfan¹⁴, C. Ivan⁸⁶, A. Ivanov¹¹⁷, V. Ivanov⁷⁶, M. Ivanov⁸⁶, O. Ivanytskyi², A. Jachołkowski³⁰, P. M. Jacobs⁶⁸, L. Jancurová⁵⁹, H.J. Jang⁶³, S. Jangal⁵⁸, R. Janik³³, M.A. Janik¹¹⁸, P.H.S.Y. Jayarathna¹¹⁰, S. Jena⁴¹, R.T. Jimenez Bustamante⁵⁵, L. Jirden³⁰, P.G. Jones⁹¹, H. Jung³⁷, W. Jung³⁷, A. Jusko⁹¹, A.B. Kaidalov⁴⁶, V. Kakoyan¹²¹, S. Kalcher³⁶, P. Kaliňák⁴⁷, M. Kalisky⁵⁴, T. Kalliokoski³⁸, A. Kalweit⁵³, K. Kanaki¹⁵, J.H. Kang¹²³, V. Kaplin⁷⁰, A. Karasu Uysal^{30,122}, O. Karavichev⁴⁴, T. Karavicheva⁴⁴, E. Karpechev⁴⁴, A. Kazantsev⁸⁹, U. Kebschull^{62,51}, R. Keidel¹²⁴, P. Khan⁹⁰, M.M. Khan¹⁴, S.A. Khan¹¹⁶, A. Khanzadeev⁷⁶, Y. Kharlov⁴³, B. Kileng³², D.J. Kim³⁸, D.W. Kim³⁷, J.H. Kim¹⁷, J.S. Kim³⁷, M. Kim¹²³, S.H. Kim³⁷, S. Kim¹⁷, T. Kim¹²³, B. Kim¹²³, S. Kirsch^{36,30}, I. Kisel³⁶, S. Kiselev⁴⁶, A. Kisiel^{30,118}, J.L. Klay⁴, J. Klein⁸³, C. Klein-Bösing⁵⁴, M. Kliemant⁵², A. Kluge³⁰, M.L. Knichel⁸⁶, K. Koch⁸³, M.K. Köhler⁸⁶, A. Kolojvari¹¹⁷, V. Kondratiev¹¹⁷, N. Kondratyeva⁷⁰, A. Konevskikh⁴⁴, A. Korneev⁸⁸, C. Kottachchi Kankanamge Don¹¹⁹, R. Kour⁹¹, M. Kowalski¹⁰⁴, S. Kox⁶⁵, G. Koyithatta Meethalevedu⁴¹, J. Kral³⁸, I. Králik⁴⁷, F. Kramer⁵², I. Kraus⁸⁶, T. Krawutschke^{83,31}, M. Krelina³⁴, M. Kretz³⁶, M. Krivda^{91,47}, F. Krizek³⁸, M. Krus³⁴, E. Kryshen⁷⁶, M. Krzewicki^{73,86}, Y. Kucheriaev⁸⁹, C. Kuhn⁵⁸, P.G. Kuijter⁷³, P. Kurashvili¹⁰¹, A. Kurepin⁴⁴, A.B. Kurepin⁴⁴, A. Kuryakin⁸⁸, V. Kuschpil⁷⁴, S. Kuschpil⁷⁴, H. Kvaerno¹⁸, M.J. Kweon⁸³, Y. Kwon¹²³, P. Ladrón de Guevara⁵⁵, I. Lakomov^{42,117}, R. Langoy¹⁵, C. Lara⁵¹, A. Lardeux¹⁰², P. La Rocca²⁴, C. Lazzeroni⁹¹, R. Lea²⁰, Y. Le Bornec⁴², K.S. Lee³⁷, S.C. Lee³⁷, F. Lefèvre¹⁰², J. Lehnert⁵², L. Leistam³⁰, M. Lenhardt¹⁰², V. Lenti⁹⁴, H. León⁵⁶, I. León Monzón¹⁰⁶, H. León Vargas⁵², P. Lévai⁶⁰, X. Li¹¹, J. Lien¹⁵, R. Lietava⁹¹, S. Lindal¹⁸, V. Lindenstruth³⁶, C. Lippmann^{86,30}, M.A. Lisa¹⁶, L. Liu¹⁵, P.I. Loenne¹⁵, V.R. Loggins¹¹⁹, V. Loginov⁷⁰, S. Lohn³⁰, D. Lohner⁸³, C. Loizides⁶⁸, K.K. Loo³⁸, X. Lopez⁶⁴, E. López Torres⁶, G. Løvnhøiden¹⁸, X.-G. Lu⁸³, P. Luettig⁵², M. Lunardon²², J. Luo⁴⁰, G. Luparello⁴⁵, L. Luquin¹⁰², C. Luzzi³⁰, K. Ma⁴⁰, R. Ma¹²⁰, D.M. Madagodahettige-Don¹¹⁰, A. Maevskaya⁴⁴, M. Mager^{53,30}, D.P. Mahapatra⁴⁸, A. Maire⁵⁸, M. Malaev⁷⁶, I. Maldonado Cervantes⁵⁵, L. Malinina^{59,ii}, D. Mal'Kevich⁴⁶, P. Malzacher⁸⁶, A. Mamonov⁸⁸, L. Manceau⁹⁵, L. Mangotra⁸¹, V. Manko⁸⁹, F. Manso⁶⁴, V. Manzari⁹⁴, Y. Mao^{65,40}, M. Marchisone^{64,26}, J. Mareš⁴⁹, G.V. Margagliotti^{20,98}, A. Margotti⁹⁶, A. Marín⁸⁶, C. Markert¹⁰⁵, I. Martashvili¹¹², P. Martinengo³⁰, M.I. Martínez¹, A. Martínez Davalos⁵⁶, G. Martínez García¹⁰², Y. Martynov², A. Mas¹⁰², S. Masciocchi⁸⁶, M. Maserà²⁶, A. Masoni⁹³, L. Massacrier^{109,102}, M. Mastromarco⁹⁴, A. Mastroserio^{28,30}, Z.L. Matthews⁹¹, A. Matyja¹⁰², D. Mayani⁵⁵, C. Mayer¹⁰⁴, J. Mazer¹¹², M.A. Mazzoni⁹⁹, F. Meddi²³, A. Menchaca-Rocha⁵⁶, J. Mercado Pérez⁸³, M. Meres³³, Y. Miake¹¹⁴, A. Michalon⁵⁸, L. Milano²⁶, J. Milosevic^{18,iii}, A. Mischke⁴⁵, A.N. Mishra⁸², D. Miśkowiec^{86,30}, C. Mitu⁵⁰, J. Mlynarz¹¹⁹, B. Mohanty¹¹⁶, A.K. Mohanty³⁰, L. Molnar³⁰, L. Montaño Zetina⁸, M. Monteno⁹⁵, E. Montes⁷, T. Moon¹²³, M. Morando²², D.A. Moreira De Godoy¹⁰⁷, S. Moretto²², A. Morsch³⁰, V. Muccifora⁶⁶, E. Mudnic¹⁰³, S. Muhuri¹¹⁶, H. Müller³⁰, M.G. Munhoz¹⁰⁷, L. Musa³⁰, A. Musso⁹⁵, B.K. Nandi⁴¹, R. Nania⁹⁶, E. Nappi⁹⁴, C. Natrass¹¹², N.P. Naumov⁸⁸, S. Navin⁹¹, T.K. Nayak¹¹⁶, S. Nazarenko⁸⁸, G. Nazarov⁸⁸, A. Nedosekin⁴⁶, M. Nicassio²⁸, B.S. Nielsen⁷², T. Niida¹¹⁴, S. Nikolaev⁸⁹, V. Nikolic⁸⁷, S. Nikulin⁸⁹, V. Nikulin⁷⁶, B.S. Nilsen⁷⁷, M.S. Nilsson¹⁸, F. Noferini^{96,9}, P. Nomokonov⁵⁹, G. Nooren⁴⁵, N. Novitzky³⁸, A. Nyanin⁸⁹, A. Nyatha⁴¹, C. Nygaard⁷², J. Nystrand¹⁵, A. Ochirov¹¹⁷, H. Oeschler^{53,30}, S. Oh¹²⁰, S.K. Oh³⁷, J. Oleniacz¹¹⁸, C. Oppedisano⁹⁵, A. Ortiz Velasquez⁵⁵, G. Ortona^{30,26}, A. Oskarsson²⁹, P. Ostrowski¹¹⁸, I. Otterlund²⁹, J. Otwinowski⁸⁶, K. Oyama⁸³, K. Ozawa¹¹³, Y. Pachmayer⁸³, M. Pachr³⁴, F. Padilla²⁶, P. Pagano²⁵, G. Paic⁵⁵, F. Painke³⁶, C. Pajares¹³, S.K. Pal¹¹⁶, S. Pal¹², A. Palaha⁹¹, A. Palmeri⁹⁷, V. Papikyan¹²¹, G.S. Pappalardo⁹⁷, W.J. Park⁸⁶, A. Passfeld⁵⁴, B. Pastirčák⁴⁷, D.I. Patalakha⁴³, V. Paticchio⁹⁴, A. Pavlinov¹¹⁹, T. Pawlak¹¹⁸, T. Peitzmann⁴⁵, M. Perales¹⁰, E. Pereira De Oliveira Filho¹⁰⁷, D. Peresunko⁸⁹, C.E. Pérez Lara⁷³, E. Perez Lezama⁵⁵, D. Perini³⁰, D. Perrino²⁸, W. Peryt¹¹⁸, A. Pesci⁹⁶, V. Peskov^{30,55}, Y. Pestov³, V. Petráček³⁴, M. Petran³⁴, M. Petris⁷¹, P. Petrov⁹¹, M. Petrovici⁷¹, C. Petta²⁴, S. Piano⁹⁸, A. Piccotti⁹⁵, M. Pikna³³, P. Pillot¹⁰², O. Pinazza³⁰, L. Pinsky¹¹⁰, N. Pitz⁵², F. Piuz³⁰, D.B. Piyarathna¹¹⁰, M. Płoskoń⁶⁸, J. Pluta¹¹⁸, T. Pocheptsov^{59,18}, S. Pochybova⁶⁰, P.L.M. Podesta-Lerma¹⁰⁶, M.G. Poghosyan^{30,26}, K. Polák⁴⁹, B. Polichtchouk⁴³, A. Pop⁷¹, S. Porteboeuf-Houssais⁶⁴, V. Pospíšil³⁴, B. Potukuchi⁸¹, S.K. Prasad¹¹⁹, R. Preghenella^{96,9}, F. Prino⁹⁵, C.A. Pruneau¹¹⁹, I. Pshenichnov⁴⁴, S. Puchagin⁸⁸, G. Puudu²¹, A. Pulvirenti^{24,30}, V. Punin⁸⁸, M. Putiš³⁵, J. Putschke^{119,120}, E. Quercigh³⁰, H. Qvigstad¹⁸, A. Rachevski⁹⁸, A. Rademakers³⁰, S. Radomski⁸³, T.S. Rähö³⁸, J. Rak³⁸, A. Rakotozafindrabe¹², L. Ramello²⁷, A. Ramírez Reyes⁸, S. Raniwala⁸², R. Raniwala⁸², S.S. Räsänen³⁸, B.T. Rascanu⁵², D. Rathee⁷⁸, K.F. Read¹¹², J.S. Real⁶⁵, K. Redlich^{101,57}, P. Reichelt⁵², M. Reicher⁴⁵, R. Renfordt⁵², A.R. Reolon⁶⁶, A. Reshetin⁴⁴, F. Rettig³⁶, J.-P. Revol³⁰, K. Reygers⁸³, L. Riccati⁹⁵, R.A. Ricci⁶⁷, T. Richert²⁹, M. Richter¹⁸, P. Riedler³⁰, W. Riegler³⁰, F. Riggi^{24,97}, M. Rodríguez Cahuanti¹, K. Røed¹⁵, D. Rohr³⁶, D. Röhrich¹⁵, R. Romita⁸⁶, F. Ronchetti⁶⁶, P. Rosnet⁶⁴, S. Rossegger³⁰, A. Rossi²², F. Roukoutakis⁷⁹, P. Roy⁹⁰, C. Roy⁵⁸,

A.J. Rubio Montero⁷, R. Rui²⁰, E. Ryabinkin⁸⁹, A. Rybicki¹⁰⁴, S. Sadovsky⁴³, K. Šafařík³⁰, P.K. Sahu⁴⁸, J. Saini¹¹⁶, H. Sakaguchi³⁹, S. Sakai⁶⁸, D. Sakata¹¹⁴, C.A. Salgado¹³, J. Salzwedel¹⁶, S. Sambyal⁸¹, V. Samsonov⁷⁶, X. Sanchez Castro^{55,58}, L. Šándor⁴⁷, A. Sandoval⁵⁶, M. Sano¹¹⁴, S. Sano¹¹³, R. Santo⁵⁴, R. Santoro^{94,30}, J. Sarkamo³⁸, E. Scapparone⁹⁶, F. Scarlassara²², R.P. Scharenberg⁸⁴, C. Schiaua⁷¹, R. Schicker⁸³, C. Schmidt⁸⁶, H.R. Schmidt^{86,115}, S. Schreiner³⁰, S. Schuchmann⁵², J. Schukraft³⁰, Y. Schutz^{30,102}, K. Schwarz⁸⁶, K. Schweda^{86,83}, G. Scioli¹⁹, E. Scomparin⁹⁵, P.A. Scott⁹¹, R. Scott¹¹², G. Segato²², I. Selyuzhenkov⁸⁶, S. Senyukov^{27,58}, J. Seo⁸⁵, S. Serici²¹, E. Serradilla^{7,56}, A. Sevcenco⁵⁰, I. Sgura⁹⁴, A. Shabetai¹⁰², G. Shabratova⁵⁹, R. Shahoyan³⁰, N. Sharma⁷⁸, S. Sharma⁸¹, K. Shigaki³⁹, M. Shimomura¹¹⁴, K. Shtejer⁶, Y. Sibiriak⁸⁹, M. Siciliano²⁶, E. Sicking³⁰, S. Siddhanta⁹³, T. Siemiarczuk¹⁰¹, D. Silvermyr⁷⁵, G. Simonetti^{28,30}, R. Singaraju¹¹⁶, R. Singh⁸¹, S. Singha¹¹⁶, T. Sinha⁹⁰, B.C. Sinha¹¹⁶, B. Sitar³³, M. Sitta²⁷, T.B. Skaali¹⁸, K. Skjerdal¹⁵, R. Smakal³⁴, N. Smirnov¹²⁰, R. Snellings⁴⁵, C. Søggaard⁷², R. Soltz⁶⁹, H. Son¹⁷, M. Song¹²³, J. Song⁸⁵, C. Soos³⁰, F. Soramel²², I. Sputowska¹⁰⁴, M. Spyropoulou-Stassinaki⁷⁹, B.K. Srivastava⁸⁴, J. Stachel⁸³, I. Stan⁵⁰, I. Stan⁵⁰, G. Stefanek¹⁰¹, G. Stefanini³⁰, T. Steinbeck³⁶, M. Steinpreis¹⁶, E. Stenlund²⁹, G. Steyn⁸⁰, D. Stocco¹⁰², M. Stolpovskiy⁴³, K. Strabykin⁸⁸, P. Strmen³³, A.A.P. Suaide¹⁰⁷, M.A. Subieta Vásquez²⁶, T. Sugitate³⁹, C. Suire⁴², M. Sukhorukov⁸⁸, R. Sultanov⁴⁶, M. Šumbera⁷⁴, T. Susa⁸⁷, A. Szanto de Toledo¹⁰⁷, I. Szarka³³, A. Szostak¹⁵, C. Tagridis⁷⁹, J. Takahashi¹⁰⁸, J.D. Tapia Takaki⁴², A. Tauro³⁰, G. Tejeda Muñoz¹, A. Telesca³⁰, C. Terrevoli²⁸, J. Thäder⁸⁶, D. Thomas⁴⁵, J.H. Thomas⁸⁶, R. Tieulent¹⁰⁹, A.R. Timmins¹¹⁰, D. Tlusty³⁴, A. Toia^{36,30}, H. Torii^{39,113}, L. Toscano⁹⁵, F. Tosello⁹⁵, T. Traczyk¹¹⁸, D. Truesdale¹⁶, W.H. Trzaska³⁸, T. Tsuji¹¹³, A. Tumkin⁸⁸, R. Turrisi¹⁰⁰, T.S. Tveter¹⁸, J. Ulery⁵², K. Ullaland¹⁵, J. Ulrich^{62,51}, A. Uras¹⁰⁹, J. Urbán³⁵, G.M. Urciuoli⁹⁹, G.L. Usai²¹, M. Vajzer^{34,74}, M. Vala^{59,47}, L. Valencia Palomo⁴², S. Vallero⁸³, N. van der Kolk⁷³, P. Vande Vyvre³⁰, M. van Leeuwen⁴⁵, L. Vannucci⁶⁷, A. Vargas¹, R. Varma⁴¹, M. Vasileiou⁷⁹, A. Vasiliev⁸⁹, V. Vechernin¹¹⁷, M. Veldhoen⁴⁵, M. Venaruzzo²⁰, E. Vercellin²⁶, S. Vergara¹, D.C. Vernekohl⁵⁴, R. Vernet⁵, M. Verweij⁴⁵, L. Vickovic¹⁰³, G. Viesti²², O. Vikhlyantsev⁸⁸, Z. Vilakazi⁸⁰, O. Villalobos Baillie⁹¹, A. Vinogradov⁸⁹, Y. Vinogradov⁸⁸, L. Vinogradov¹¹⁷, T. Virgili²⁵, Y.P. Viyogi¹¹⁶, A. Vodopyanov⁵⁹, S. Voloshin¹¹⁹, K. Voloshin⁴⁶, G. Volpe^{28,30}, B. von Haller³⁰, D. Vranic⁸⁶, G. Øvrebeck¹⁵, J. Vrláková³⁵, B. Vulpescu⁶⁴, A. Vyushin⁸⁸, B. Wagner¹⁵, V. Wagner³⁴, R. Wan^{58,40}, Y. Wang⁸³, M. Wang⁴⁰, D. Wang⁴⁰, Y. Wang⁴⁰, K. Watanabe¹¹⁴, J.P. Wessels^{30,54}, U. Westerhoff⁵⁴, J. Wiechula^{83,115}, J. Wikne¹⁸, M. Wilde⁵⁴, G. Wilk¹⁰¹, A. Wilk⁵⁴, M.C.S. Williams⁹⁶, B. Windelband⁸³, L. Xaplanteris Karampatsos¹⁰⁵, H. Yang¹², S. Yang¹⁵, S. Yasnopolskiy⁸⁹, J. Yi⁸⁵, Z. Yin⁴⁰, H. Yokoyama¹¹⁴, I.-K. Yoo⁸⁵, J. Yoon¹²³, W. Yu⁵², X. Yuan⁴⁰, I. Yushmanov⁸⁹, C. Zach³⁴, C. Zampolli^{96,30}, S. Zaporozhets⁵⁹, A. Zarochentsev¹¹⁷, P. Závada⁴⁹, N. Zaviyalov⁸⁸, H. Zbroszczyk¹¹⁸, P. Zelnicsek^{30,51}, I.S. Zgura⁵⁰, M. Zhalov⁷⁶, X. Zhang^{64,40}, F. Zhou⁴⁰, D. Zhou⁴⁰, Y. Zhou⁴⁵, X. Zhu⁴⁰, A. Zichichi^{19,9}, A. Zimmermann⁸³, G. Zinovjev², Y. Zoccarato¹⁰⁹, M. Zynovyev²

Affiliation notes

- ⁱ Deceased
- ⁱⁱ Also at: M.V.Lomonosov Moscow State University, D.V.Skobeltzyn Institute of Nuclear Physics, Moscow, Russia
- ⁱⁱⁱ Also at: "Vinča" Institute of Nuclear Sciences, Belgrade, Serbia

Collaboration Institutes

- ¹ Benemérita Universidad Autónoma de Puebla, Puebla, Mexico
- ² Bogolyubov Institute for Theoretical Physics, Kiev, Ukraine
- ³ Budker Institute for Nuclear Physics, Novosibirsk, Russia
- ⁴ California Polytechnic State University, San Luis Obispo, California, United States
- ⁵ Centre de Calcul de l'IN2P3, Villeurbanne, France
- ⁶ Centro de Aplicaciones Tecnológicas y Desarrollo Nuclear (CEADEN), Havana, Cuba
- ⁷ Centro de Investigaciones Energéticas Medioambientales y Tecnológicas (CIEMAT), Madrid, Spain
- ⁸ Centro de Investigación y de Estudios Avanzados (CINVESTAV), Mexico City and Mérida, Mexico
- ⁹ Centro Fermi – Centro Studi e Ricerche e Museo Storico della Fisica "Enrico Fermi", Rome, Italy
- ¹⁰ Chicago State University, Chicago, United States
- ¹¹ China Institute of Atomic Energy, Beijing, China
- ¹² Commissariat à l'Energie Atomique, IRFU, Saclay, France

- ¹³ Departamento de Física de Partículas and IGFAE, Universidad de Santiago de Compostela, Santiago de Compostela, Spain
- ¹⁴ Department of Physics Aligarh Muslim University, Aligarh, India
- ¹⁵ Department of Physics and Technology, University of Bergen, Bergen, Norway
- ¹⁶ Department of Physics, Ohio State University, Columbus, Ohio, United States
- ¹⁷ Department of Physics, Sejong University, Seoul, South Korea
- ¹⁸ Department of Physics, University of Oslo, Oslo, Norway
- ¹⁹ Dipartimento di Fisica dell'Università and Sezione INFN, Bologna, Italy
- ²⁰ Dipartimento di Fisica dell'Università and Sezione INFN, Trieste, Italy
- ²¹ Dipartimento di Fisica dell'Università and Sezione INFN, Cagliari, Italy
- ²² Dipartimento di Fisica dell'Università and Sezione INFN, Padova, Italy
- ²³ Dipartimento di Fisica dell'Università 'La Sapienza' and Sezione INFN, Rome, Italy
- ²⁴ Dipartimento di Fisica e Astronomia dell'Università and Sezione INFN, Catania, Italy
- ²⁵ Dipartimento di Fisica 'E.R. Caianiello' dell'Università and Gruppo Collegato INFN, Salerno, Italy
- ²⁶ Dipartimento di Fisica Sperimentale dell'Università and Sezione INFN, Turin, Italy
- ²⁷ Dipartimento di Scienze e Tecnologie Avanzate dell'Università del Piemonte Orientale and Gruppo Collegato INFN, Alessandria, Italy
- ²⁸ Dipartimento Interateneo di Fisica 'M. Merlin' and Sezione INFN, Bari, Italy
- ²⁹ Division of Experimental High Energy Physics, University of Lund, Lund, Sweden
- ³⁰ European Organization for Nuclear Research (CERN), Geneva, Switzerland
- ³¹ Fachhochschule Köln, Köln, Germany
- ³² Faculty of Engineering, Bergen University College, Bergen, Norway
- ³³ Faculty of Mathematics, Physics and Informatics, Comenius University, Bratislava, Slovakia
- ³⁴ Faculty of Nuclear Sciences and Physical Engineering, Czech Technical University in Prague, Prague, Czech Republic
- ³⁵ Faculty of Science, P.J. Šafárik University, Košice, Slovakia
- ³⁶ Frankfurt Institute for Advanced Studies, Johann Wolfgang Goethe-Universität Frankfurt, Frankfurt, Germany
- ³⁷ Gangneung-Wonju National University, Gangneung, South Korea
- ³⁸ Helsinki Institute of Physics (HIP) and University of Jyväskylä, Jyväskylä, Finland
- ³⁹ Hiroshima University, Hiroshima, Japan
- ⁴⁰ Hua-Zhong Normal University, Wuhan, China
- ⁴¹ Indian Institute of Technology, Mumbai, India
- ⁴² Institut de Physique Nucléaire d'Orsay (IPNO), Université Paris-Sud, CNRS-IN2P3, Orsay, France
- ⁴³ Institute for High Energy Physics, Protvino, Russia
- ⁴⁴ Institute for Nuclear Research, Academy of Sciences, Moscow, Russia
- ⁴⁵ Nikhef, National Institute for Subatomic Physics and Institute for Subatomic Physics of Utrecht University, Utrecht, Netherlands
- ⁴⁶ Institute for Theoretical and Experimental Physics, Moscow, Russia
- ⁴⁷ Institute of Experimental Physics, Slovak Academy of Sciences, Košice, Slovakia
- ⁴⁸ Institute of Physics, Bhubaneswar, India
- ⁴⁹ Institute of Physics, Academy of Sciences of the Czech Republic, Prague, Czech Republic
- ⁵⁰ Institute of Space Sciences (ISS), Bucharest, Romania
- ⁵¹ Institut für Informatik, Johann Wolfgang Goethe-Universität Frankfurt, Frankfurt, Germany
- ⁵² Institut für Kernphysik, Johann Wolfgang Goethe-Universität Frankfurt, Frankfurt, Germany
- ⁵³ Institut für Kernphysik, Technische Universität Darmstadt, Darmstadt, Germany
- ⁵⁴ Institut für Kernphysik, Westfälische Wilhelms-Universität Münster, Münster, Germany
- ⁵⁵ Instituto de Ciencias Nucleares, Universidad Nacional Autónoma de México, Mexico City, Mexico
- ⁵⁶ Instituto de Física, Universidad Nacional Autónoma de México, Mexico City, Mexico
- ⁵⁷ Institut of Theoretical Physics, University of Wrocław
- ⁵⁸ Institut Pluridisciplinaire Hubert Curien (IPHC), Université de Strasbourg, CNRS-IN2P3, Strasbourg, France
- ⁵⁹ Joint Institute for Nuclear Research (JINR), Dubna, Russia
- ⁶⁰ KFKI Research Institute for Particle and Nuclear Physics, Hungarian Academy of Sciences, Budapest, Hungary
- ⁶¹ Kharkiv Institute of Physics and Technology (KIPT), National Academy of Sciences of Ukraine (NASU),

- Kharkov, Ukraine
- 62 Kirchhoff-Institut für Physik, Ruprecht-Karls-Universität Heidelberg, Heidelberg, Germany
- 63 Korea Institute of Science and Technology Information
- 64 Laboratoire de Physique Corpusculaire (LPC), Clermont Université, Université Blaise Pascal, CNRS–IN2P3, Clermont-Ferrand, France
- 65 Laboratoire de Physique Subatomique et de Cosmologie (LPSC), Université Joseph Fourier, CNRS-IN2P3, Institut Polytechnique de Grenoble, Grenoble, France
- 66 Laboratori Nazionali di Frascati, INFN, Frascati, Italy
- 67 Laboratori Nazionali di Legnaro, INFN, Legnaro, Italy
- 68 Lawrence Berkeley National Laboratory, Berkeley, California, United States
- 69 Lawrence Livermore National Laboratory, Livermore, California, United States
- 70 Moscow Engineering Physics Institute, Moscow, Russia
- 71 National Institute for Physics and Nuclear Engineering, Bucharest, Romania
- 72 Niels Bohr Institute, University of Copenhagen, Copenhagen, Denmark
- 73 Nikhef, National Institute for Subatomic Physics, Amsterdam, Netherlands
- 74 Nuclear Physics Institute, Academy of Sciences of the Czech Republic, Řež u Prahy, Czech Republic
- 75 Oak Ridge National Laboratory, Oak Ridge, Tennessee, United States
- 76 Petersburg Nuclear Physics Institute, Gatchina, Russia
- 77 Physics Department, Creighton University, Omaha, Nebraska, United States
- 78 Physics Department, Panjab University, Chandigarh, India
- 79 Physics Department, University of Athens, Athens, Greece
- 80 Physics Department, University of Cape Town, iThemba LABS, Cape Town, South Africa
- 81 Physics Department, University of Jammu, Jammu, India
- 82 Physics Department, University of Rajasthan, Jaipur, India
- 83 Physikalisches Institut, Ruprecht-Karls-Universität Heidelberg, Heidelberg, Germany
- 84 Purdue University, West Lafayette, Indiana, United States
- 85 Pusan National University, Pusan, South Korea
- 86 Research Division and ExtreMe Matter Institute EMMI, GSI Helmholtzzentrum für Schwerionenforschung, Darmstadt, Germany
- 87 Rudjer Bošković Institute, Zagreb, Croatia
- 88 Russian Federal Nuclear Center (VNIIEF), Sarov, Russia
- 89 Russian Research Centre Kurchatov Institute, Moscow, Russia
- 90 Saha Institute of Nuclear Physics, Kolkata, India
- 91 School of Physics and Astronomy, University of Birmingham, Birmingham, United Kingdom
- 92 Sección Física, Departamento de Ciencias, Pontificia Universidad Católica del Perú, Lima, Peru
- 93 Sezione INFN, Cagliari, Italy
- 94 Sezione INFN, Bari, Italy
- 95 Sezione INFN, Turin, Italy
- 96 Sezione INFN, Bologna, Italy
- 97 Sezione INFN, Catania, Italy
- 98 Sezione INFN, Trieste, Italy
- 99 Sezione INFN, Rome, Italy
- 100 Sezione INFN, Padova, Italy
- 101 Soltan Institute for Nuclear Studies, Warsaw, Poland
- 102 SUBATECH, Ecole des Mines de Nantes, Université de Nantes, CNRS-IN2P3, Nantes, France
- 103 Technical University of Split FESB, Split, Croatia
- 104 The Henryk Niewodniczanski Institute of Nuclear Physics, Polish Academy of Sciences, Cracow, Poland
- 105 The University of Texas at Austin, Physics Department, Austin, TX, United States
- 106 Universidad Autónoma de Sinaloa, Culiacán, Mexico
- 107 Universidade de São Paulo (USP), São Paulo, Brazil
- 108 Universidade Estadual de Campinas (UNICAMP), Campinas, Brazil
- 109 Université de Lyon, Université Lyon 1, CNRS/IN2P3, IPN-Lyon, Villeurbanne, France
- 110 University of Houston, Houston, Texas, United States
- 111 University of Technology and Austrian Academy of Sciences, Vienna, Austria
- 112 University of Tennessee, Knoxville, Tennessee, United States
- 113 University of Tokyo, Tokyo, Japan

- ¹¹⁴ University of Tsukuba, Tsukuba, Japan
- ¹¹⁵ Eberhard Karls Universität Tübingen, Tübingen, Germany
- ¹¹⁶ Variable Energy Cyclotron Centre, Kolkata, India
- ¹¹⁷ V. Fock Institute for Physics, St. Petersburg State University, St. Petersburg, Russia
- ¹¹⁸ Warsaw University of Technology, Warsaw, Poland
- ¹¹⁹ Wayne State University, Detroit, Michigan, United States
- ¹²⁰ Yale University, New Haven, Connecticut, United States
- ¹²¹ Yerevan Physics Institute, Yerevan, Armenia
- ¹²² Yildiz Technical University, Istanbul, Turkey
- ¹²³ Yonsei University, Seoul, South Korea
- ¹²⁴ Zentrum für Technologietransfer und Telekommunikation (ZTT), Fachhochschule Worms, Worms, Germany